analytical chemistry

Article

Cite This: *Anal. Chem.* 2019, 91, 6027−6034

pubs.acs.org/ac

Filter Beacon: A Gating-Free Architecture for Protein-Specific Glycoform Imaging on Cell Surface

Yiran Liu, Lu Liu, Siqiao Li, Guyu Wang, Huangxian Ju, and Lin Ding*

State Key Laboratory of Analytical Chemistry for Life Science, School of Chemistry and Chemical Engineering, Nanjing University, Nanjing 210023, P. R. China

Supporting Information

ABSTRACT: The imaging characterization of spatial proximity of covalently linked structural motifs (e.g., protein-specific glycoform) is essential for thorough understanding of cellular chemistry and biology. The current imaging formats rely on gating-based mechanisms for generating correct closed-loop signaling topology, and they can suffer from low signal intensity, restricted applicability, and complicated design. We report herein the development of a mechanistically distinct filter beacon architecture for protein-specific glycoform imaging on the cell surface. The elaborate structuring of molecular beacon segment, nicking restriction site, and docking moiety lays out a general nongated design principle for passing through intended closed-loop signaling topology and sifting out false-positive open-loop leakage topology, furnishing a straightforward imaging format with high signal intensity and broad applicability. Proof-of-concept protocols have been developed for the imaging of MUC1-bound terminal sialic acid and fucose. The versatile adaptability of the protocols also enables dynamic monitoring of protein-specific glycosylation pattern changes in response to the alteration of cellular physiological states. Given the convenience for achieving multiplexed encoding and decoding, through fluorescence signals alone or together with filter beacon sequences, the filter beacon architecture should permit comprehensive imaging of diverse-structured carbohydrates on a given glycoprotein.

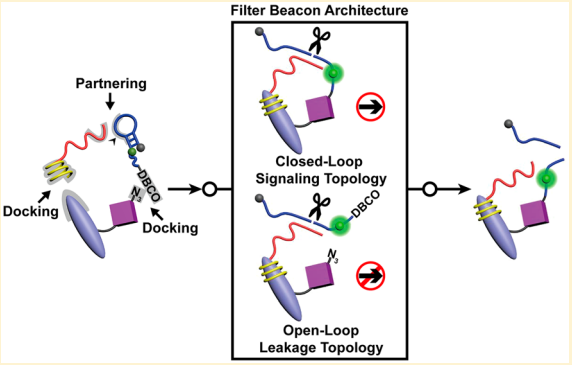

Protein glycosylation is a conserved and essential post-translational modification that allows the vast expansion of proteomic diversity.[1] The glycosylation pattern, or glycoform, characteristic of a particular protein is under the delicate control of coordinated cellular enzymatic actions[2] and governs a protein's folding, stability, trafficking,[3] as well as the host cell's recognition and signaling properties.[4] The nontemplate nature of the glycosylation process translates to transient and dynamic fingerprinting-level structural adaptivity to both cellular physiological states and environmental cues.[5,6] In situ protein-specific glycoform imaging can therefore not only provide insight into glycosylation pathways and functions[7−15] but also contribute to the identification of diagnostic and therapeutic targets.[16]

The imaging characterization of spatial proximity of covalently connected structural motifs (e.g., protein-specific glycoforms) requires the creation of closed-loop signaling topology and elimination of open-loop leakage topology; topology is used herein to refer to the fundamental mathematical invariant feature of an imaging protocol irrespective of the physical, chemical, or biological nature of the implementation process. The closed-loop signaling topology refers to the correct signaling topological configuration formed by the full bridging of structural motifs of interest (e.g., protein and carbohydrate) with a spectrum of intermediate constructs; the constructs can be created based on the docking of probe units (e.g., DNA probe strands), via affinity binding (e.g., aptamer binding) or covalent bonding (e.g., click chemistry), and partnering of probe units (e.g., DNA probe hybridization); this is the proper topological configuration for signaling because of the precise structural motif identity encoding through probe docking and subsequent identity decoding signaling through probe partnering. The open-loop leakage topology refers to the incorrect topological configuration formed by the partial bridging of structural motifs of interest, such as when the docking of one probe unit (e.g., DNA probe strand for the carbohydrate) fails; this is the erroneous topological configuration because of the loss of identity information for one structural motif (e.g., carbohydrate) and faulty generation of false-positive leakage signal. All the protein-specific glycoform imaging strategies developed thus far use gating, referred to herein as a control scheme where the docking of probe units occurs before the proximity partnering of probe units, as a safeguard mechanism to ensure the exclusive intraglycoprotein-confined formation of closed-loop signaling topology.[7−15] The Förster resonance energy transfer (FRET) scheme relies on distance as the gating

Received: January 31, 2019
Accepted: April 17, 2019
Published: April 17, 2019

DOI: 10.1021/acs.analchem.9b00551
Anal. Chem. 2019, 91, 6027−6034

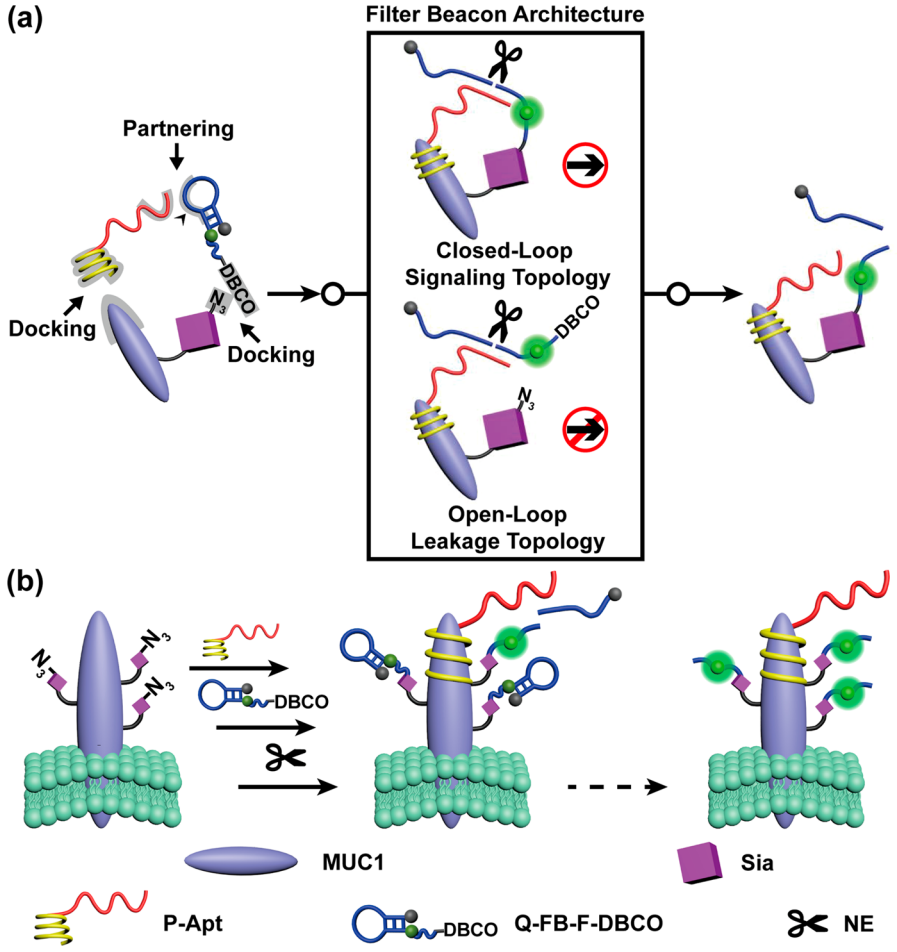

Figure 1. Schematic illustration of the filter beacon architecture (a) for protein-specific glycoform imaging on cell surface (b).

handle.[7−11] The localized chemical remodeling (LCM) method exploits ions as the gating media.[12] The hierarchical coding (HieCo) approach applies DNA-gating as the control channel.[13] These strategies can suffer from various drawbacks, including low sensitivity (FRET), restricted applicability (LCM), and complicated design (HieCo). A fundamental paradigm shift is therefore in urgent need for the achievement of high signal intensity and broad applicability with a simplified, gating-free architecture.

We report herein the development of a filter beacon architecture for protein-specific glycoform imaging on the cell surface (Figure 1). The filter beacon architecture refers to a nongated, molecular beacon-based signal-filtering platform that relies on a nicking endonuclease (NE) nicking action to pass through the correct intraglycoprotein-confined closed-loop signaling topology and sift out the incorrect open-loop leakage topology; this can be likened to an electronic filter that only passes through signals within a desired frequency range and sifts out signals outside the designated window. In particular, the filter beacon acts as a probe unit on the carbohydrate side and features three key design elements, (1) a hairpin-shaped DNA molecular beacon segment containing a fluorophore and a quencher at the opposite ends of stem region,[17] (2) a nicking restriction site spanning the loop and stem regions, (3) a docking moiety linked through a spacer segment to the fluorophore-side stem end. The probe unit on the protein side comprises a DNA segment complementary to part of the filter beacon (in both the loop region and stem region), a spacer, and a docking moiety. The imaging operation proceeds via (1) metabolic engineering incorporation of a reactive moiety on a carbohydrate site;[18] (2) docking of the protein-targeting probe unit; (3) docking of the carbohydrate-targeting filter beacon intertwined with both closed-loop signaling topology- and open-loop leakage topology-forming hybridization of probe units; and (4) nicking cleavage of the hybridized filter beacon, resulting in dehybridization-enabled retention of closed-loop signaling topology (with signaling fluorophore attached to the carbohydrate site) and removal of open-loop leakage topology (with signaling fluorophore liberated into the solution). The released protein-targeting probe unit is then available for the next round of a closed loop topology-signaling, proximity hybridization−cleavage−dehybridization catalytic reaction with a docked folded filter beacon.

The elimination of open-loop leakage topology has been a persistently challenging issue for nongated detection of protein-specific glycoforms. The substantial lowering of a probe unit concentration can be employed for prioritizing the occurrence of docking over a partnering event and therefore formation of a closed-loop signaling topology, but this maneuver renders it impossible to perform an imaging operation due to the insufficient amount of installed probe units.[19] The filter beacon architecture allows its essentially unconstrained high concentration usage at the docking/hybridization stage and subsequent catalytic turnover generation of plentiful intended signaling entities in the carbohydrate-bound state, thus offering high signal intensity.

DOI: 10.1021/acs.analchem.9b00551
Anal. Chem. 2019, 91, 6027−6034

In addition, through our straightforward, nongated imaging architecture, the carbohydrate identity can be traced either simply with a fluorophore fluorescence signal or together with filter beacon DNA sequence, thus guaranteeing broad carbohydrate applicability. In fact, a significant advantage of our method is the ability to use a single filter beacon DNA sequence for the highly effective identification of multiple types of carbohydrates, as long as mutually orthogonal docking reactions and fluorescence signals are brought in place for encoding and decoding, due to the persistent covalent locking of fluorophores onto respective carbohydrates throughout the imaging process.

EXPERIMENTAL SECTION

Materials and Reagents. Fetal bovine serum (FBS), orange DNA loading dye (6×), SYBR gold nucleic acid gel stain (10 000×), Click-iT tetraacetylated *N*-azidoacetyl-D-mannosamine (Ac_4ManNAz, for the metabolic engineering incorporation of azide-modified sialic acid, or azide-modified Sia, onto the cell surface), Click-iT tetraacetylfucose alkyne (Ac_4FucAl, for the metabolic engineering incorporation of alkyne-modified Fuc onto cell surface), lipofectamine 3000 transfection reagent, Opti-MEM, RIPA lysis and extraction buffer, Halt protease inhibitor cocktail (100×), NuPAGE LDS sample buffer (4×), and PageRuler prestained protein ladder (10 to 180 kDa) were purchased from Thermo Fisher Scientific Inc. (USA). Ammonium persulfate, Tris-HCl/SDS buffer (4×, pH 6.8), Tris-HCl/SDS buffer (4×, pH 8.8), TBS buffer (20×), Tris-glycine gel running buffer (10×, pH 8.3), and Western transfer buffer (10×) were obtained from Shanghai Sangon Biotech. Inc. (China). PBS buffer (pH 7.4, containing 136.7 mM NaCl, 2.7 mM KCl, 8.72 mM Na_2HPO_4, 1.41 mM KH_2PO_4, 1 mM $CaCl_2$, and 1 mM $MgCl_2$); RPMI-1640; Dulbecco's modified eagle's medium (DMEM); MCF-7; T47D; HepG2 cell lines; and two plasmids, shRNA and shRNA-NC, were supplied by KeyGen Biotech Co., Ltd. (China). Methanol, bovine serum albumin (BSA), ethylenediaminetetraacetic acid (EDTA), *N*,*N*,*N*′,*N*′-tetramethylethylenediamine (TEMED), Tris, (+)-sodium L-ascorbate, copper(II) sulfate pentahydrate ($CuSO_4{\cdot}5H_2O$), TWEEN 20, and boric acid were obtained from Sigma-Aldrich Inc. (USA). Benzyl-2-acetamido-2-deoxy-α-D-galactopyranoside (BAG) was purchased from Santa Cruz Biotechnology Inc. (USA). AccuWest ECL Blaster Western blotting HRP substrate was purchased from Bioelite Co., Ltd. (China). α2-3,6,8,9-Neuraminidase (NEU), GlycoBuffer (10×), NE (Nt.BbvCI), and Cutsmart buffer (10×) were purchased from New England Biolabs (USA). Anti-MUC1 antibody, anti-GAPDH antibody, and tunicamycin (TM) were obtained from Abcam PLC Co., Ltd. (USA). HRP conjugated goat anti-rabbit IgG and BSA blocking buffer were purchased from Cwbio Co., Ltd. (China). Insulin was obtained from Yeasen Co., Ltd. (China). 2-(4-((Bis((1-(*tert*-butyl)-1*H*-1,2,3-triazol-4-yl)-methyl)amino)-methyl)-1*H*-1,2,3-triazol-1-yl) acetic acid (BTTAA) was obtained from Click Chemistry Tools, LLC (USA). All aqueous solutions were prepared using ultrapure water (≥18 MΩ, Milli-Q, Millipore).

In Vitro Polyacrylamide Gel Electrophoresis (PAGE) Analysis. The **FB** strand (all DNA sequences read from 5′ to 3′, and for details, refer to Table S1; **FB** denotes the filter beacon sequence as the carbohydrate-targeting probe unit, and for the detailed description of DNA sequence design, refer to the Results and Discussion section) was first thermally annealed in PBS (5 min heating at 95 °C, then 0.5 °C/min cooling to 25 °C) to form a stable hairpin structure. In the first set of experiments, four samples containing **P-Apt** (**P** denotes the MUC1-targeting probe unit DNA sequence; **Apt** denotes the MUC1-binding aptamer sequence, S2.2[20]) and annealed **FB** were prepared in 1× Cutsmart buffer, 1 μM **P-Apt**; 1 μM **FB**; a mixture of 1 μM **P-Apt** and 1 μM **FB**; and a mixture of 1 μM **P-Apt**, 1 μM **FB**, and 1000 U/mL NE. All the samples were incubated at 37 °C for 1.5 h. In addition, a mixture of 1 μM **P-Apt** and 1 μM **FB** was directly incubated in PBS. In the second set of experiments, six samples containing **P-Apt** and annealed **FB** were prepared in 1× Cutsmart buffer, 1 μM **P-Apt**; 1 μM **FB**; 200 nM **FB**; a mixture of 1 μM **P-Apt** and 1 μM **FB**; a mixture of 1 μM **P-Apt** and 200 nM **FB**; and a mixture of 1 μM **P-Apt**, 1 μM **FB**, and 1000 U/mL NE. All the samples were incubated at 37 °C for 1.5 h. To verify the specificity of the enzyme, 1 μM **P-Apt** and 1 μM **FB** were individually treated at 37 °C with 1000 U/mL NE for 1.5 h. To investigate the effect of temperature, a mixture of 1 μM **P-Apt** and 1 μM **FB** and a mixture of 1 μM **P-Apt** and 200 nM **FB** were incubated at 4 °C for 1.5 h. In yet another set of experiments, a mixture of 1 μM **P-Apt** and 1 μM **FB** and a mixture of 1 μM **P-Apt** and 200 nM **FB** were directly incubated in PBS. After the incubation step, 10 μL of each sample was mixed with 2 μL 6× loading buffer. Then, 3 μL of each of the mixtures was injected into 12% polyacrylamide hydrogel. Electrophoresis was performed at 100 V in 1× TBE buffer for 70 min. The hydrogel was then immersed in the 1× SYBR gold dye (dilution of 10 000× dye into 1× TBE buffer), and the staining was allowed to proceed at room temperature (r.t.) on a shaker for 30 min. The stained hydrogel was then photographed under UV irradiation.

In Vitro Fluorescence Analysis. **P-Apt** and **Q-FB-F** (**Q** denotes the quencher DABCYL; **F** denotes the fluorophore FAM) (fixed at 100 nM) were mixed in 0.1:1, 1:1, and 5:1 ratios in PBS. The mixture was incubated at 4 °C for 30 min. A pure **Q-FB-F** sample undergoing an identical incubation procedure was used as a control. The set of experiments were analogously performed at 4 and 37 °C in 1× Cutsmart buffer for 1.5 h. To verify the feasibility of achieving a hybridization−cleavage−dehybridization catalysis, a mixture of **P-Apt** (10 nM), **Q-FB-F** (100 nM), and 250 U/mL NE was incubated at 37 °C in 1× Cutsmart buffer for 1.5 h. The fluorescence spectra of these samples were then measured. The excitation wavelength and emission wavelength were set at 494 and 518 nm, respectively. The excitation and emission slits were set at 5.0 and 10.0 nm, respectively. The photomultiplier tube voltage used was 750 V.

Confocal Laser Scanning Microscope (CLSM) Imaging of P-Apt Binding to MUC1. The MCF-7 cells and HepG2 cells were seeded on the 4-well confocal dishes and cultured in a 37 °C incubator containing 5% CO_2 for 12 h. The cells were then incubated in 40 μM 10% FBS-containing RPMI-1640 solution of metabolic reagent Ac_4ManNAz for 48 h for the metabolic engineering incorporation of the azide group onto Sia. The cells were washed three times with 1% FBS-containing PBS (note, washing was used after every cell manipulation step in all the following experiments). To block nonspecific interaction, the cells were incubated at 4 °C with 1% FBS-containing PBS for 30 min. The cells were then incubated at 4 °C with 1 μM PBS solution of either **F-P-Apt** or **F-P-Ran** (**Ran** denotes a random DNA sequence) for 30 min. The cells were fixed by immersion at r.t. in 4% formaldehyde solution for

DOI: 10.1021/acs.analchem.9b00551
Anal. Chem. 2019, 91, 6027−6034

15 min and immediately imaged by CLSM. The fluorescence signal from 495 to 550 nm was collected under 488 nm excitation.

Click Chemistry. The docking of **Q-FB-F-DBCO** (**DBCO** denotes dibenzocyclooctyne) and **FB-F-DBCO** was achieved through Cu(I)-free click chemistry. The cells were incubated in 40 μM 10% FBS-containing RPMI-1640 solution of metabolic reagent Ac_4ManNAz for 48 h for the metabolic engineering incorporation of the azide group onto Sia. Then, 10 μM PBS solution of either **Q-FB-F-DBCO** or **FB-F-DBCO** was added and allowed to react at 4 °C with metabolically engineered cells for 30 min. The docking of **Q-FB-F-N_3** (**N_3** denotes azide) was achieved through Cu(I)-catalyzed click chemistry. The cells were incubated in 40 μM 10% FBS-containing RPMI-1640 solution of metabolic reagent Ac_4FucAl for 48 h for the metabolic engineering incorporation of alkyne group onto Fuc. Then, a 0.5% FBS-containing PBS solution, including 100 μM $CuSO_4{\cdot}5H_2O$, 600 μM BTTAA, 10 μM **Q-FB-F-N_3**, and 2.5 mM (+)-sodium L-ascorbate, was added and allowed to react at r.t. with metabolically engineered cells for 5 min.

Filter Beacon Imaging Optimization of Nicking Cleavage Reaction. The MCF-7 cells were seeded on the 4-well confocal dishes and cultured at 37 °C for 12 h. Metabolic engineering was performed by incubating the cells at 37 °C with 40 μM Ac_4ManNAz for 48 h. After the blocking of the nonspecific interaction, the cells were incubated at 4 °C with 1 μM PBS solution of **P-Apt** for 30 min. Then, a 10 μM PBS solution of **Q-FB-F-DBCO** was added and allowed to react at 4 °C with metabolically engineered cells for 30 min. The cells were then fixed. One group of cells were incubated for 1.5 h with different concentrations of NE, and the other group of cells were incubated with 600 U/mL NE for different durations of time.

Filter Beacon Imaging of Protein-Specific Glycoform. The cells were seeded on the 4-well confocal dishes and cultured at 37 °C for 12 h. The cells were then incubated with a 40 μM 10% FBS-containing RPMI-1640 solution of metabolic reagent (either Ac_4ManNAz or Ac_4FucAl) for 48 h. After the nonspecific interaction was blocked, the cells were incubated at 4 °C with 1 μM PBS solution of **P-Apt** for 30 min. Then, a 10 μM PBS solution of **Q-FB-F-DBCO** (for the Ac_4ManNAz batch) or **Q-FB-F-N_3** (for the Ac_4FucAl batch) was allowed to react at 4 °C with metabolically engineered cells for 30 min. The cells were then fixed. The cells underwent a nicking cleavage reaction at 37 °C with 600 U/mL NE for 1.5 h and were immediately subjected to CLSM imaging.

Filter Beacon Imaging after Inhibition of Glycosylation Processes. The MCF-7 cells were seeded on the 4-well confocal dishes and cultured at 37 °C for 12 h. The cells were then incubated with either a mixture of 40 μM Ac_4ManNAz and 2.5 μM *O*-glycosylation inhibitor BAG or a mixture of 40 μM Ac_4ManNAz and 1 μM *N*-glycosylation inhibitor TM for 48 h. The subsequent steps were identical to those used in the Filter Beacon Imaging of Protein-Specific Glycoform section. The effect of glycosylation inhibition on the expression level of MUC1 was probed by incubation of the above metabolically engineered, glycosylation-inhibited MCF-7 cells at 4 °C with **F-P-Apt** for 30 min and quantification of the fluorescence signal intensity with CLSM imaging.

Filter Beacon Imaging after NEU Treatment. The MCF-7 cells were seeded on the 4-well confocal dishes and cultured at 37 °C for 12 h. The cells were then incubated in a 40 μM 10% FBS-containing RPMI-1640 solution of metabolic reagent Ac_4ManNAz for 48 h and further treated at 37 °C with 0.2 U/mL 1× GlycoBuffer solution of NEU for 1 h. The subsequent steps were identical to those used in the Filter Beacon Imaging of Protein-Specific Glycoform section.

CLSM Imaging of MUC1 upon Plasmid Transfection. After the transfection of shRNA or shRNA-NC, the MCF-7 cells were digested by trypsin, seeded on the four-well confocal dishes, and cultured for 12 h. A sample without plasmid transfection was used as a control. The subsequent steps were identical to those used, with **F-P-Apt** as the probe, in the Confocal Laser Scanning Microscope (CLSM) Imaging of **P-Apt** Binding to MUC1 section.

Filter Beacon Imaging upon Plasmid Transfection. After the transfection of shRNA or shRNA-NC, the MCF-7 cells were digested by trypsin, seeded on the four-well confocal dishes, and cultured for 12 h. A sample without plasmid transfection was used as a control. The subsequent steps were identical to those used in the Filter Beacon Imaging of Protein-Specific Glycoform section.

Validation of Removal of Open-Loop Leakage Topology. The MCF-7 cells were seeded on the 4-well confocal dishes and cultured at 37 °C for 12 h. One group of cells were metabolically engineered with Ac_4ManNAz, and the other group of cells were not. The metabolically engineered cells were incubated at 4 °C with 1 μM **P-Apt** for 30 min, followed by incubation at 4 °C with 10 μM **Q-FB-F** for 30 min. After the fixation, the cells were either treated at 37 °C with 600 U/mL NE for 1.5 h or incubated at 37 °C in 1× Cutsmart buffer for 1.5 h. The other group of cells (without undergoing metabolic engineering process) were first incubated at 4 °C with 1 μM **P-Apt** for 30 min and then incubated at 4 °C with 10 μM **Q-FB-F-DBCO** for 30 min. After the fixation, the cells were either treated at 37 °C with 600 U/mL NE for 1.5 h or incubated at 37 °C in 1× Cutsmart buffer for 1.5 h. The cells were then imaged by CLSM.

RESULTS AND DISCUSSION

Probe Units for Filter Beacon Architecutre. For the proof-of-concept demonstration of filter beacon imaging, MUC1-bound terminal sialic acid (Sia) is selected as the initial target. MUC1 is a transmembrane glycoprotein characterized by a unique extracellular domain of heavily *O*-glycosylated variable number tandem repeats (VNTR).[21] MUC1 plays an important role in cell adhesion, signal transduction, and cancer metastasis, and it is a highly discriminatory theranostic biomarker.[22] Sia serves as a critical mediator for cell recognition, neuronal development, and pathogen infection.[23] For MUC1-specific terminal Sia imaging, a designer Sia-targeting 37mer filter beacon probe, **Q-FB-F-DBCO**, is fabricated and contains the as-stated three requisite elements, (1) a 31mer molecular beacon segment, including a 20mer loop region, a two 5mer stem region, a fluorophore FAM located on a nucleotide adjacent to the 3′-end of stem region, and a quencher DABCYL located at the 5′-end of stem region; (2) a 7mer NE Nt.BbvCI nicking restriction site[24] (6 in the loop region and 1 in the stem region) flanked by a 4mer on the 5′ side (loop region) and a nucleotide on the 3′ side (stem region), constituting a 12mer sequence complementary to a 12mer segment of protein-targeting probe unit, **P-Apt**; and (3) a dibenzocyclooctyne (DBCO) docking moiety (for strain-promoted Cu(I)-free click reaction with azide)[25] conjugated through a 6mer spacer to the FAM-carrying nucleotide. **P-Apt**

DOI: 10.1021/acs.analchem.9b00551
Anal. Chem. 2019, 91, 6027−6034

contains, starting from the 5′-end, a 12mer hybridization sequence, a consecutive flexible spacer of 16mer and hexaethylene glycol, and a 25mer high-affinity MUC1 VNTR-binding docking aptamer, S2.2.[20]

In Vitro Verification of the Working Principle of Filter Beacon Architecture. Key to the successful implementation of the filter beacon imaging architecture is the ability to achieve both a highly effective nicking cleavage of **Q-FB-F-DBCO** upon hybridization with **P-Apt** and highly efficient dehybridization release of catalytic **P-Apt** after cleavage. The hybridization−cleavage−dehybridization catalysis is first evaluated in vitro by native PAGE on a system containing **FB** and the pure 12mer hybridization sequence from **P** (**P-12**). As expected, thermodynamics (predicted melting temperature for **P-Apt**/**FB**, 46.2 °C; measured value, 43.0 °C, vide infra) only allows for the partial attainment of the hybridization state at either 37 °C or under a thermal annealing condition (Figure S1, lanes 1−4). The NE nicking action on the **P-12**/**FB** duplex offers a thermodynamically downhill dehybridization path for the full cleavage of **FB** and leaves the catalytic species **P-12** intact (Figure S1, lanes 4 and 5). Partial hybridization is beneficial for diminishing the probability of open-loop leakage topology formation at the probe unit docking stage, while the full cleavage of **FB** guarantees the sufficiency of the probe unit partnering-generated closed-loop topology signaling entities for readout. The switching from **P-12** to the full-length **P-Apt** retains the essentially identical partial hybridization capability with **FB** (slight upward shifting of **P-Apt** band and weakening of **FB** band intensity) in a temperature-independent manner (at 4 or 37 °C, or with thermal annealing) (Figure S2, lanes 4−9), confirming that the spacer and aptamer portions of the sequence do not interfere with the hybridization process. The nicking cleavage is not observed for either single-stranded **P-Apt** or folded **FB** (Figure 2a, lanes 1−4) but is fully effective

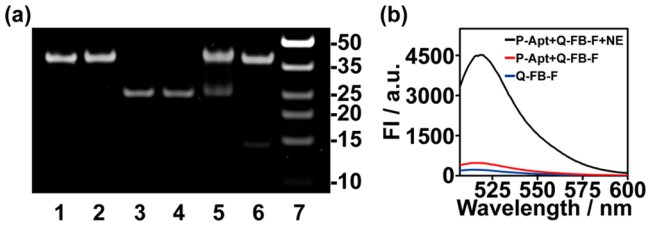

Figure 2. In vitro demonstration of the working principle of filter beacon architecture. (a) Native PAGE analysis of a system of **P-Apt** (1 μM), **FB** (1 μM), and NE (1000 U/mL). (Lane 1) **P-Apt**; (2) **P-Apt** and NE; (3) **FB**; (4) **FB** and NE; (5) **P-Apt** and **FB**; (6) **P-Apt**, **FB**, and NE; and (7) DNA ladder. (b) Fluorescence analysis of a system of **Q-FB-F** (100 nM), **P-Apt** (10 nM), and NE (250 U/mL). All are incubated at 37 °C in 1× Cutsmart buffer for 1.5 h.

on **FB** for the **P-Apt**/**FB** duplex (Figure 2a, lanes 5 and 6). To better monitor the hybridization and nicking cleavage processes, FAM is conjugated to either **FB** (as **FB-F**) or **P-Apt** (as **F-P-Apt**) for tracking the behavior of each individual strand. Direct visualization identifies two otherwise elusive observations (Figure S3), the predominance of folded **FB** over the duplexed form, consistent with partial hybridization (lanes 1, 2, 4, 5), and the complete retention of **P-Apt** and complete cleavage of **FB** (in originally both the folded and duplexed forms; lanes 2, 3, 5, and 6), consistent with hybridization−cleavage−dehybridization catalysis. The partial hybridization and nicking cleavage are also supported by a fluorescence measurement on the system of **P-Apt** and **Q-FB-F**. Thus, the opening of the hairpin from the folded state and accompanied restoration of fluorescence from the quenched state for **Q-FB-F** can occur only partially, in a **P-Apt** quantity- and time-dependent, temperature-independent manner (Figure S4). The addition of NE leads to the full operation of the hybridization−cleavage−dehybridization catalytic cycle and complete recovery of fluorescence (Figure 2b).

The 5mer stem sequence and 12mer hybridization sequence employed herein provide the properly balanced catalysis-enabling structure, a too stable stem (e.g., via lengthening of the stem region) leads to less efficient hybridization and nicking cleavage; similarly, a too weak hybridization strength (e.g., via shortening of the hybridization sequence) implies less efficient nicking cleavage. A too strong hybridization strength (e.g., via increase of the GC content of hybridization sequence) causes less efficient dehybridization and turnover after nicking cleavage.

Protein-Specific Glycoform Imaging on Cell Surface. With the crucial catalytic nicking cleavage feature demonstrated in vitro for the filter beacon, we proceed to the examination of its applicability to the imaging of the MUC1-specific terminal Sia on the cell surface. CLSM shows that **P-Apt** docking on MUC1 is highly effective through the binding of the aptamer segment (Figure S5), and a fluorescence signal can be immediately observed on an MUC1-positive MCF-7 cell surface upon incubation at 4 °C with **F-P-Apt** for 30 min; the high degree of the aptamer sequence specificity requirement for binding is evidenced by the absence of the fluorescence signal on the MCF-7 cell surface when switching to **F-P-Ran**, a DNA strand with the aptamer portion of **F-P-Apt** replaced by a random-sequenced DNA. The MUC1-targeting specificity is supported by failed binding of **F-P-Apt** (as well as **F-P-Ran**) on the MUC1-negative HepG2 cell surface.[26] The docking of the filter beacon on the MCF-7 cell surface can be effected through initial metabolic engineering incorporation of an azide group onto Sia and the subsequent Cu(I)-free click reaction with the DBCO moiety (Figure S6), and no fluorescence signal can be identified in the absence of either the azide group (with **FB-F** or **FB-F-DBCO**) or the DBCO moiety (with or without azide; with **FB-F**); fluorescence signal is apparent after a 4 °C, 30 min click reaction between the Sia azide and **FB-F-DBCO**.

With the docking capability of both probe units individually validated, the feasibility of performing the MUC1-specific terminal Sia imaging on MCF-7 cell surface is examined. Imaging can indeed be achieved with the following protocol (Figures 3, S7, and S8),metabolic engineering installation of the azide group on Sia, blocking of the nonspecific interaction by incubation of MCF-7 cells at 4 °C in 1% FBS-containing 1× phosphate buffer saline (PBS, pH 7.4) for 30 min, docking of **P-Apt** by incubation at 4 °C for 30 min, docking/hybridization of **Q-FB-F-DBCO** by incubation at 4 °C for 30 min, cell fixation at room temperature for 15 min, and 37 °C treatment with NE.

The generation of closed-loop topology signaling entities and elimination of open-loop leakage topology both critically rely on the nicking cleavage action from NE. The amount of NE and duration of the nicking action therefore require optimization in reference to the fluorescence signal intensity that can be generated after execution of the imaging protocol. The fluorescence signal intensity reaches the plateau upon the 1.5 h treatment with 600 U/mL NE (Figures S7 and S8).

DOI: 10.1021/acs.analchem.9b00551
Anal. Chem. 2019, 91, 6027−6034

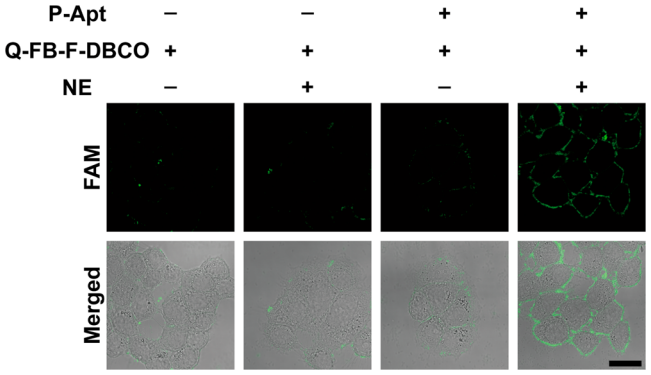

Figure 3. Filter beacon imaging of MUC1-bound terminal Sia on MCF-7 cell surface. CLSM imaging of MCF-7 cells after metabolic engineering incorporation of Sia azide and further treatments with **P-Apt**, **Q-FB-F-DBCO**, and NE. Scale bar, 25 μm.

Significantly, the optimized imaging protocol allows for efficient removal of open-loop leakage topology (Figure 4),

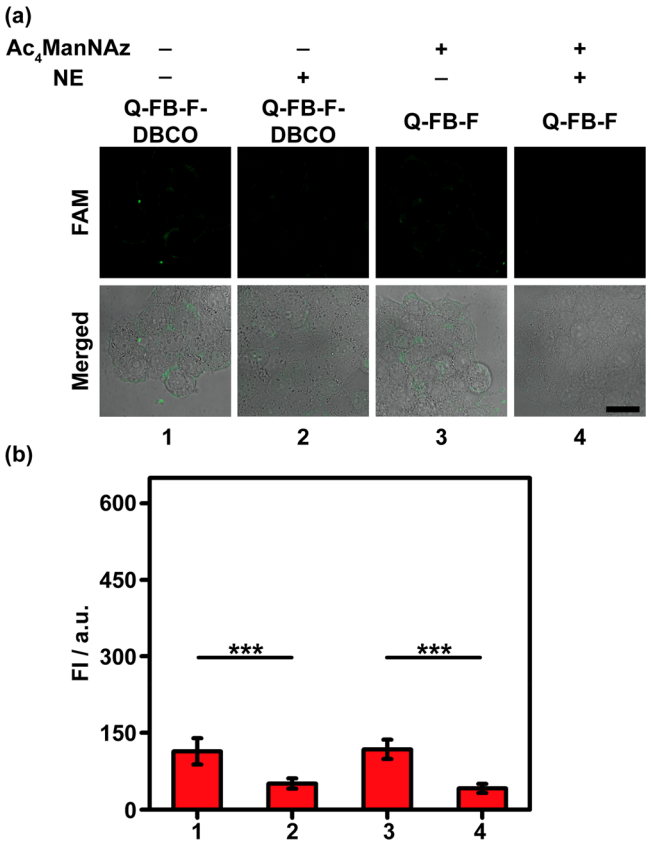

Figure 4. CLSM imaging demonstrating the ability of filter beacon architecture to remove open-loop leakage topology. (a) CLSM imaging of MCF-7 cells (without or with metabolic engineering incorporation of Sia azide) after **P-Apt** docking and incubation with **Q-FB-F-DBCO** or **Q-FB-F**, before and after the nicking action from NE. (b) Fluorescence signal intensity before and after the nicking action. Scale bar, 25 μm. For fluorescence signal intensity measurement, 10 cells are used. Statistical analysis, *t*-test (***$p < 0.001$). There is no docking of **Q-FB-F-DBCO** or **Q-FB-F** on the MCF-7 cell surface because of the lack of either Sia azide or DBCO. Residual fluorescence signal from the hybridization of **P-Apt** with solution-state **Q-FB-F-DBCO** or **Q-FB-F** (open-loop leakage topology signal) can be efficiently removed by the NE nicking action.

and residual fluorescence signal observed on the MCF-7 cell surface (without azide) after **P-Apt** docking and further hybridization with **FB-F-DBCO** (signifying low hybridization efficiency, consistent with in vitro results) can be substantially attenuated with nicking cleavage. Similarly, residual hybridization between **P-Apt** and **FB-F** (with the azide on MCF-7 cell surface) can be largely eliminated with nicking cleavage.

Further systematic studies indicate that the MUC1-specific terminal Sia imaging operates in accordance with the working principle of the filter beacon architecture (Figure 3), and the docking of **Q-FB-F-DBCO** on the Sia azide retains its fully folded hairpin state, thus exhibiting a minimum background-level fluorescence signal; the nicking action is not effective on the docked folded **Q-FB-F-DBCO**, and only residual hybridization occurs between **Q-FB-F-DBCO** and **P-Apt** at the **Q-FB-F-DBCO** docking stage. The nicking action can initiate the full proximity hybridization−cleavage−dehybridization catalytic cycle for docked **P-Apt** and **Q-FB-F-DBCO**, providing a tremendously increased fluorescence signal for MUC1-specific terminal Sia imaging. Comparison of the fluorescence signals generated by **F-P-Apt** binding and filter beacon architecture indicates an average turnover number of 2.4. Note, that the DNA sequences have not been optimized herein, and an increase of the turnover number is expected once optimized.

Validation of Protein-Specific Glycoform Imaging Target. To further validate the confinement of imaging specifically to the MUC1-bound terminal Sia, three sets of experiments are undertaken. MUC1 is exclusively *O*-glycosylated,[21] and as a result, the imaging signal intensity will be negatively influenced only by the inhibition of *O*-linked glycosylation but not *N*-linked glycosylation. The rationale is supported by the observation of vastly diminished imaging signal intensity in response to benzyl 2-acetamido-2-deoxy-α-D-galactopyranoside (BAG, an inhibitor for *O*-linked glycosylation)[27] treatment and essentially identical imaging signal intensity when exposed to tunicamycin (TM, an inhibitor for N-linked glycosylation) (Figure 5a,b).[28] In addition, the direct impact on the expression level of MUC1 from BAG and TM can be excluded based on the quantitative imaging of MUC1 with **F-P-Apt** (Figure S9). The MUC1-targeting specificity is further evidenced by the decrease of the imaging signal intensity (Figures 5c,d and S10a) accompanying the knockdown of the MUC1 expression level by shRNA (Figure S11)[29] (as quantitatively assessed by Western blot analysis and **F-P-Apt** imaging, Figure S12). The terminal Sia-targeting specificity is confirmed by the significant lowering of imaging signal intensity upon the trimming of terminal Sia with NEU (Figures 5e,f and S10b).[30] Collectively, the imaging target specificity verification experiments conclusively show that the filter beacon imaging architecture can also be used for monitoring the dynamic change of glycosylation patterns for a specific glycoprotein with the alteration of cellular physiological states, subjected to both internal (disruption of *O*-linked glycosylation pathways and down-regulation of MUC1 expression level) and external (enzymatic trimming of terminal Sia) disturbances.

Demonstration of the Versatile Applicability in Protein-Specific Glycoform Imaging. The filter beacon architecture is designed to be a versatile imaging platform with broad carbohydrate applicability. To verify the flexible adaptability imaging feature, MUC1-bound terminal fucose (Fuc) on the MCF-7 cell surface[31] and MUC1-bound terminal Sia on the T47D cell surface[31,32] are selected as the

DOI: 10.1021/acs.analchem.9b00551
Anal. Chem. 2019, 91, 6027−6034

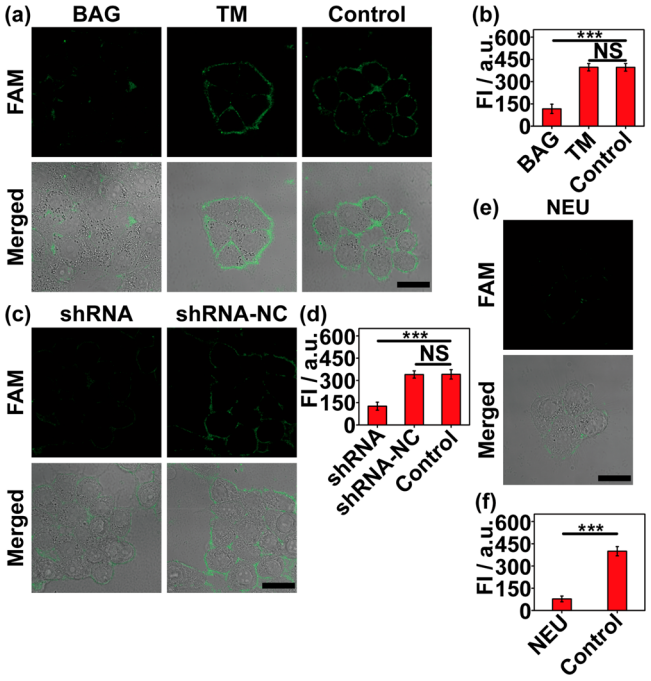

Figure 5. Demonstration of filter beacon imaging specificity of MUC1-bound terminal Sia. (a) Filter beacon imaging of MCF-7 cells under BAG and TM treatments. Control, no treatment. (b) Fluorescence signal intensity from (a). (c) Filter beacon imaging of MCF-7 cells after transfection with shRNA (shRNA-NC, control plasmid). (d) Fluorescence signal intensity from (c) and Figure S10a. (e) Filter beacon imaging of MCF-7 cells after NEU treatment. (f) Fluorescence signal intensity from (e) and Figure S10b. Scale bars, 25 μm. Statistical analysis, *t*-test (***p < 0.001; NS, not significant).

demonstration targets. For the former target, metabolic engineering incorporation of an alkyne group onto Fuc is used for the docking of **Q-FB-F-N_3** through an orthogonal Cu(I)-catalyzed click reaction with the azide moiety. For the latter target, an otherwise identical protocol for imaging of the MUC1-bound terminal Sia is adopted, except with the replacement of MCF-7 cells by T47D cells. The imaging of both targets can be, as expected, efficiently achieved (Figure 6).

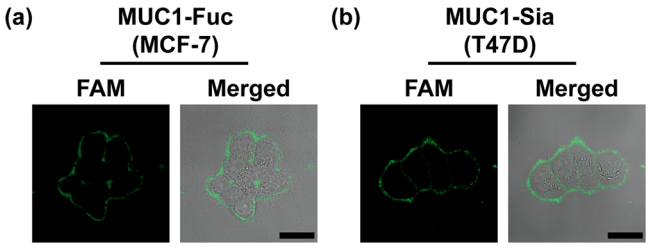

Figure 6. Filter beacon imaging of MUC1-bound terminal Fuc on MCF-7 cell surface (a) and MUC1-bound terminal Sia on T47D cell surface (b). Scale bar, 25 μm.

CONCLUSION

In conclusion, we have proposed herein a nongated, mechanistically distinct filter beacon architecture and demonstrated its utility in protein-specific glycoform imaging on the cell surface. The elaborate structuring of the molecular beacon segment, nicking restriction site, and docking moiety allows for highly effective differentiation between correct closed-loop signaling topology and false-positive open-loop leakage topology. Proof-of-concept imaging has been demonstrated for MUC1-bound terminal Sia and Fuc. Given the convenience for achieving multiplexed encoding and decoding, via fluorescence signals alone or together with filter beacon sequences, the filter beacon architecture should enable comprehensive imaging of diverse-structured carbohydrates on a given glycoprotein.

ASSOCIATED CONTENT

Supporting Information

The Supporting Information is available free of charge on the ACS Publications website at DOI: 10.1021/acs.analchem.9b00551.

Additional experimental section, DNA sequence information, native PAGE analysis, fluorescence analysis, CLSM imaging, requirements of engineering incorporation, optimization, and a vector map (PDF)

AUTHOR INFORMATION

Corresponding Author

*Phone/Fax: +86-25-89681927; E-mail: dinglin@nju.edu.cn.

ORCID

Huangxian Ju: 0000-0002-6741-5302

Lin Ding: 0000-0001-5381-3484

Notes

The authors declare no competing financial interest.

ACKNOWLEDGMENTS

We gratefully acknowledge support from the National Natural Science Foundation of China (21675082), the National Key Research and Development Program of China (2018YFC1004704), Fundamental Research Funds for the Central Universities (020514380184), and State Key Laboratory of Analytical Chemistry for Life Science (5431ZZXM1903).

REFERENCES

(1) Varki, A. *Glycobiology* **2017**, *27*, 3−49.
(2) Bard, F.; Chia, J. *Trends Cell Biol.* **2016**, *26*, 379−388.
(3) Xu, C.; Ng, D. T. *Nat. Rev. Mol. Cell Biol.* **2015**, *16*, 742−752.
(4) Macauley, M. S.; Crocker, P. R.; Paulson, J. C. *Nat. Rev. Immunol.* **2014**, *14*, 653−666.
(5) Paszek, M. J.; DuFort, C. C.; Rossier, O.; Bainer, R.; Mouw, J. K.; Godula, K.; Hudak, J. E.; Lakins, J. N.; Wijekoon, A. C.; Cassereau, L.; Rubashkin, M. G.; Magbanua, M. J.; Thorn, K. S.; Davidson, M. W.; Rugo, H. S.; Park, J. W.; Hammer, D. A.; Giannone, G.; Bertozzi, C. R.; Weaver, V. M. *Nature* **2014**, *511*, 319−325.
(6) Dalziel, M.; Crispin, M.; Scanlan, C. N.; Zitzmann, N.; Dwek, R. A. *Science* **2014**, *343*, 1235681.
(7) Haga, Y.; Ishii, K.; Hibino, K.; Sako, Y.; Ito, Y.; Taniguchi, N.; Suzuki, T. *Nat. Commun.* **2012**, *3*, 907.
(8) Belardi, B.; de la Zerda, A.; Spiciarich, D. R.; Maund, S. L.; Peehl, D. M.; Bertozzi, C. R. *Angew. Chem., Int. Ed.* **2013**, *52*, 14045−14049.
(9) Lin, W.; Du, Y.; Zhu, Y.; Chen, X. *J. Am. Chem. Soc.* **2014**, *136*, 679−687.
(10) Wu, N.; Bao, L.; Ding, L.; Ju, H. *Angew. Chem., Int. Ed.* **2016**, *55*, 5220−5224.
(11) Doll, F.; Buntz, A.; Späte, A. K.; Schart, V. F.; Timper, A.; Schrimpf, W.; Hauck, C. R.; Zumbusch, A.; Wittmann, V. *Angew. Chem., Int. Ed.* **2016**, *55*, 2262−2266.
(12) Hui, J.; Bao, L.; Li, S.; Zhang, Y.; Feng, Y.; Ding, L.; Ju, H. *Angew. Chem., Int. Ed.* **2017**, *56*, 8139−8143.

DOI: 10.1021/acs.analchem.9b00551
Anal. Chem. 2019, 91, 6027−6034

(13) Li, S.; Liu, Y.; Liu, L.; Feng, Y.; Ding, L.; Ju, H. *Angew. Chem., Int. Ed.* **2018**, *57*, 12007−12011.
(14) For a recent highlight of our work, please see: Suzuki, T. *Nature* **2018**, *561*, 38−40.
(15) For a recent account of our systematic efforts in cellular glycan analysis, please see: Chen, Y.; Ding, L.; Ju, H. *Acc. Chem. Res.* **2018**, *51*, 890−899.
(16) Zuegg, J.; Muldoon, C.; Adamson, G.; McKeveney, D.; Le Thanh, G.; Premraj, R.; Becker, B.; Cheng, M.; Elliott, A. G.; Huang, J. X.; Butler, M. S.; Bajaj, M.; Seifert, J.; Singh, L.; Galley, N. F.; Roper, D. I.; Lloyd, A. J.; Dowson, C. G.; Cheng, T.-J.; Cheng, W.-C.; Demon, D.; Meyer, E.; Meutermans, W.; Cooper, M. A. *Nat. Commun.* **2015**, *6*, 7719.
(17) Wang, K.; Tang, Z.; Yang, C. J.; Kim, Y.; Fang, X.; Li, W.; Wu, Y.; Medley, C. D.; Cao, Z.; Li, J.; Colon, P.; Lin, H.; Tan, W. *Angew. Chem., Int. Ed.* **2009**, *48*, 856−870.
(18) Palaniappan, K. K.; Bertozzi, C. R. *Chem. Rev.* **2016**, *116*, 14277−14306.
(19) Robinson, P. V.; de Almeida-Escobedo, G.; de Groot, A. E.; McKechnie, J. L.; Bertozzi, C. R. *J. Am. Chem. Soc.* **2015**, *137*, 10452−10455.
(20) Ferreira, C. S. M.; Matthews, C. S.; Missailidis, S. *Tumor Biol.* **2006**, *27*, 289−301.
(21) Martínez-Sáez, N.; Peregrina, J. M.; Corzana, F. *Chem. Soc. Rev.* **2017**, *46*, 7154−7175.
(22) Finn, O. J.; Gantt, K. R.; Lepisto, A. J.; Pejawar-Gaddy, S.; Xue, J.; Beatty, P. L. *Immunol. Res.* **2011**, *50*, 261−268.
(23) Büll, C.; Stoel, M. A.; den Brok, M. H.; Adema, G. J. *Cancer Res.* **2014**, *74*, 3199−3204.
(24) Lu, L.; Chan, D. S.-H.; Kwong, D. W. J.; He, H.-Z.; Leung, C.-H.; Ma, D.-L. *Chem. Sci.* **2014**, *5*, 4561−4568.
(25) Gordon, C. G.; Mackey, J. L.; Jewett, J. C.; Sletten, E. M.; Houk, K. N.; Bertozzi, C. R. *J. Am. Chem. Soc.* **2012**, *134*, 9199−9208.
(26) Yu, C.; Hu, Y.; Duan, J.; Yuan, W.; Wang, C.; Xu, H.; Yang, X.-D. *PLoS One* **2011**, *6*, e24077.
(27) Paszkiewicz-Gadek, A.; Porowska, H.; Lemancewicz, D.; Wolczynski, S.; Gindzienski, A. *Int. J. Mol. Med.* **2006**, *17*, 669−674.
(28) Wyszynski, F. J.; Lee, S. S.; Yabe, T.; Wang, H.; Gomez-Escribano, J. P.; Bibb, M. J.; Lee, S. J.; Davies, G. J.; Davis, B. G. *Nat. Chem.* **2012**, *4*, 539−546.
(29) Sachdeva, M.; Mo, Y.-Y. *Cancer Res.* **2010**, *70*, 378−387.
(30) Miyagi, T.; Takahashi, K.; Hata, K.; Shiozaki, K.; Yamaguchi, K. *Glycoconjugate J.* **2012**, *29*, 567−577.
(31) Müller, S.; Hanisch, F. G. *J. Biol. Chem.* **2002**, *277*, 26103−26112.
(32) Storr, S. J.; Royle, L.; Chapman, C. J.; Hamid, U. M. A.; Robertson, J. F.; Murray, A.; Dwek, R. A.; Rudd, P. M. *Glycobiology* **2008**, *18*, 456−462.

DOI: 10.1021/acs.analchem.9b00551
Anal. Chem. 2019, 91, 6027−6034